Nanoscale Radiative Heat Transfer and its applications

Philippe Ben-Abdallah, Svend-Age Biehs, Rosa Felipe S.S.

0

Nanoscale Radiative Heat Transfer and its Applications

Svend-Age Biehs[1], Philippe Ben-Abdallah[2] and Felipe S.S. Rosa[2]
[1]*Institut für Physik, Carl von Ossietzky Universität Oldenburg, D-26111 Oldenburg*
[2]*Laboratoire Charles Fabry, Institut d'Optique, CNRS, Université Paris-Sud, Campus Polytechnique, RD128, 91127 Palaiseau Cedex*
[1]*Germany*
[2]*France*

1. Introduction

Heat radiation at the nanoscale is a relatively young but flourishing research field, that has attracted much attention in the last decade. This is on the one hand due to the fact that this effect is nowadays experimentally accessible (Hu et al. (2008); Kittel et al (2005); Narayanaswamy et al. (2008); Ottens et al. (2011); Rousseau et al. (2009); Shen et al. (2009)), and on the other hand due to the unusual properties of thermal radiation at nanometric distances, which makes it highly promising for future applications in nanotechnology. Among these near-field properties (i.e., properties at distances smaller than the thermal wavelength), we can mention: (i) the energy exchange is not limited by the well-known Stefan-Boltzmann law for black bodies and in fact can be several orders of magnitude larger, (ii) thermal radiation at nanoscale is quasi monochromatic and (iii) it can be spatially strongly correlated despite the fact that thermal radiation is often taken as a textbook example for uncorrelated light, which is only true for distances larger than the thermal wavelength (Carminati and Greffet (1999); Polder and Van Hove (1971); Shchegrov et al (2000)). For some recent reviews see Refs. (Basu et al. (2009); Dorofeyev and Vinogradov (2011); Joulain et al. (2005); Vinogradov and Dorofeyev (2009); Volokitin and Persson (2007); Zhang (2007)).

Before we discuss possible applications exploiting the above mentioned thermal near-field properties, we first want to give a concise description of the physical origin of the electromagnetic fields radiated from the surface of a hot material within the framework of fluctutational electrodynamics. Based on this formal framework we derive the heat flux expression between two isotropic semi-infinite nonmagnetic media separated at a given distance by a vacuum gap. By means of this expression we discuss the modes which contribute to the heat flux in different distance regimes. In particular, we discuss the dominant contribution of the coupled surface modes at the nanoscale and illustrate the specific properties (i) and (ii) with some numerical results. Finally, we reformulate the heat flux expression in the same manner as it is done for the electronic transport at a mesoscopic scale (Datta (2002); Imry (2002)).

1.1 Fluctuating electrodynamics

Let's first consider a given medium at a fixed temperature T. We choose a volume $\mathcal{V}$ of this medium such that it is large compared to the size of the constituents of the material, i.e., the electrons, atoms or ions, but small on a macroscopic length scale as for example the size of the considered medium. Then the macroscopic electromagnetic fields $\mathbf{E}$, $\mathbf{D}$, $\mathbf{B}$ and $\mathbf{H}$ fullfilling the macroscopic Maxwell equations (Jackson (1998))

$$\nabla \cdot \mathbf{D}(\mathbf{r},t) = \rho^{\mathrm{e}}(\mathbf{r},t) \qquad \text{and} \qquad \nabla \times \mathbf{E}(\mathbf{r},t) = -\frac{\partial \mathbf{H}(\mathbf{r},t)}{\partial t}, \tag{1}$$

$$\nabla \cdot \mathbf{B}(\mathbf{r},t) = 0 \qquad \text{and} \qquad \nabla \times \mathbf{H}(\mathbf{r},t) = \mathbf{j}^{\mathrm{e}}(\mathbf{r},t) + \frac{\partial \mathbf{D}(\mathbf{r},t)}{\partial t} \tag{2}$$

can be regarded as the volume average over such a volume (Russakoff (1970)). Here ρ^{e} and $\mathbf{j}^{\mathrm{e}}$ are external charges or currents, respectively. Within this macroscopic or continuum description, the material properties can be described by a permittivity tensor ϵ_{ij} and a permeability tensor μ_{ij} with $i,j = 1,2,3$ relating the fields $\mathbf{D}$ and $\mathbf{E}$ and $\mathbf{B}$ and $\mathbf{H}$. When introducing the Fourier components as

$$\tilde{\mathbf{E}}(\mathbf{r},\omega) = \int_{-\infty}^{\infty} \mathrm{d}t\, \mathrm{e}^{\mathrm{i}\omega t}\mathbf{E}(\mathbf{r},t)\,, \qquad \tilde{\mathbf{H}}(\mathbf{r},\omega) = \int_{-\infty}^{\infty} \mathrm{d}t\, \mathrm{e}^{\mathrm{i}\omega t}\mathbf{H}(\mathbf{r},t)\,, \qquad \text{etc.,} \tag{3}$$

then we can write $\tilde{\mathbf{D}} = \epsilon_0 \boldsymbol{\epsilon} \cdot \tilde{\mathbf{E}}$ and $\tilde{\mathbf{B}} = \mu_0 \boldsymbol{\mu} \cdot \tilde{\mathbf{H}}$. Here, ϵ_0 and μ_0 are the permittivity and the permeability of the vacuum. In the following we are only interested in non-magnetic materials so that $\tilde{\boldsymbol{\mu}}$ is given by the unit tensor, i.e., we have $\mathbf{B} = \mu_0 \mathbf{H}$. Note, that here we have already neglected any spatial dispersion of the permittivity, which can play an important role in the near-field of metals (Chapuis et al. (2008); Ford and Weber (1984); Joulain and Henkel (2006)).

Within a neutral material there are no external charges and currents, but the random thermal motion of the constituents of matter, i.e., of the electrons, atoms or ions, induces within the average volume $\mathcal{V}$ a macroscopic fluctuating charge density ρ^{f} and a current $\mathbf{j}^{\mathrm{f}}$, which replace the external charges and currents in Maxwell's equations (1) and (2) and therefore generate fluctuating electromagnetic fields $\mathbf{E}^{\mathrm{f}}$ and $\mathbf{H}^{\mathrm{f}}$, which are now considered to be random processes as well as ρ^{f} and $\mathbf{j}^{\mathrm{f}}$. Since the latter are the sum of many microscopic random charges and currents inside the average volume $\mathcal{V}$, we can apply the *central limit theorem* and infer that these fluctuating quantities are Gaussian distributed (Kubo et al. (1991)). That means that all higher moments of these quantities are determined by their mean value and variance. This statement is also true for the fluctuating fields, because there exists a linear relation between the electromagnetic fields and the generating currents which can be stated as

$$\tilde{\mathbf{E}}^{\mathrm{f}}(\mathbf{r},\omega) = \mathrm{i}\omega\mu_0 \int_V \mathrm{d}\mathbf{r}'' \mathbb{G}^{\mathrm{E}}(\mathbf{r},\mathbf{r}'',\omega) \cdot \tilde{\mathbf{j}}^{\mathrm{f}}(\mathbf{r}'',\omega), \tag{4}$$

$$\tilde{\mathbf{H}}^{\mathrm{f}}(\mathbf{r},\omega) = \mathrm{i}\omega\mu_0 \int_V \mathrm{d}\mathbf{r}'' \mathbb{G}^{\mathrm{H}}(\mathbf{r},\mathbf{r}'',\omega) \cdot \tilde{\mathbf{j}}^{\mathrm{f}}(\mathbf{r}'',\omega), \tag{5}$$

where the integrals are taken over the volume V which contains the fluctuating source currents; $\mathbb{G}^{\mathrm{E}}$ and $\mathbb{G}^{\mathrm{H}}$ are the classical dyadic electric and magnetic Green's functions (Chen-To Tai (1971)).

By assuming that due to the thermal motion no charges will be created or destroyed we have $\langle \rho^{\mathrm{f}} \rangle = 0$, where the brackets symbolize the ensemble average. If we now further assume that

the mean fluctuating currents are vanishing in average, i.e., $\langle \mathbf{j}^{\mathrm{f}} \rangle = \mathbf{0}$, then we find that $\langle \mathbf{E}^{\mathrm{f}} \rangle = \langle \mathbf{H}^{\mathrm{f}} \rangle = \mathbf{0}$ so that in average the fields do no work on external charges or currents. In order to complete the framework of fluctuating electrodynamics first developed by Rytov (Rytov et al. (1989)) we have to specify the second moment, i.e., the correlation function of the fluctuating currents or charges. In fluctuating electrodynamics this correlation function is specified by the *fluctuation dissipation theorem* and reads (Lifshitz and Pitaevskii (2002))

$$\langle \tilde{j}_i^{\mathrm{f}}(\mathbf{r},\omega)\tilde{j}_j^{\mathrm{f}}(\mathbf{r}',\omega')\rangle = 2\pi\omega\Theta(\omega,T)\left[\tilde{\epsilon}_{ij}(\omega)-\tilde{\epsilon}_{ji}^{*}(\omega)\right]\delta(\omega-\omega')\delta(\mathbf{r}-\mathbf{r}'). \tag{6}$$

The delta-function $\delta(\mathbf{r}-\mathbf{r}')$ shows up because we have neglected spatial dispersion. The second delta function $\delta(\omega-\omega')$ reflects the fact that we have a stationary situation. Indeed, the fluctuation dissipation theorem is only valid in thermal equilibrium so that by applying this theorem we have assumed that the medium containing the fluctuating currents is in thermal equilibrium at temperature T. The function

$$\Theta(\omega,T) = \frac{\hbar\omega}{2} + \frac{\hbar\omega}{\mathrm{e}^{\hbar\omega/(k_{\mathrm{B}}T)}-1} \tag{7}$$

is the mean energy of a harmonic oscillator in thermal equilibrium and consists of the vacuum and the thermal part; k_{B} is Boltzmann's and $2\pi\hbar$ is Planck's constant. From the appearance of $\hbar$ in $\Theta(\omega,T)$ it becomes obvious that the fluctuation dissipation theorem is in principle a quantum mechanical relation. Hence, fluctuating electrodynamics combines the classical stochastic electromagnetic fields with the quantum mechanical fluctuation dissipation theorem and has therefore to be considered as a semi-classical approach (Rosa et al. (2010)).

Equipped with the correlation function for the source currents in Eq. (6) and the linear relations in Eqs. (4) and (5) we can now determine the correlation functions of the electromagnetic fields $\langle \tilde{E}_i^{\mathrm{f}}(\mathbf{r},\omega)\tilde{E}_j^{\mathrm{f}}(\mathbf{r}',\omega')\rangle$, $\langle \tilde{H}_i^{\mathrm{f}}(\mathbf{r},\omega)\tilde{H}_j^{\mathrm{f}}(\mathbf{r}',\omega')\rangle$, and $\langle \tilde{E}_i^{\mathrm{f}}(\mathbf{r},\omega)\tilde{H}_j^{\mathrm{f}}(\mathbf{r}',\omega')\rangle$ in terms of the Green's functions. Hence, if we know the classical electromagnetic Green's functions $\mathbb{G}^{\mathrm{E}}$ and $\mathbb{G}^{\mathrm{H}}$ for a given geometry we can evaluate the correlation functions of the fields allowing for determining for example Casimir forces or heat fluxes. Although some purely quantum mechanical approaches exist (Agarwal (1975); Janowicz et al. (2003); Lifshitz and Pitaevskii (2002)) fluctuating electrodynamics has the advantage of being conceptionally simple while giving the correct results for the correlation functions of the fields.

1.2 Heat flux expression

Now we want to determine the heat flux between two semi-infinite media (see Fig. 1) which are at local thermal equilibrium and have the temperatures T_1 and T_2. We assume that both media are separated by a vacuum gap of thickness d. In order to determine the heat flux, we first consider $T_2 = 0$ so that we consider only fluctuating currents $\mathbf{j}_1^{\mathrm{f}}$ in medium 1. The fluctuating fields $\mathbf{E}_1^{\mathrm{f}}$ and $\mathbf{H}_1^{\mathrm{f}}$ inside the vacuum gap generated by the fluctuating sources in medium 1 can be expressed in terms of the relations (4) and (5). From these expressions one can determine the mean Poynting vector in z direction

$$\langle S_z^{1\to 2}\rangle = \langle \mathbf{E}_1^{\mathrm{f}} \times \mathbf{H}_1^{\mathrm{f}}\rangle \cdot \mathbf{e}_z \tag{8}$$

by means of the fluctuation dissipation theorem in Eq. (6). The resulting expression contains the dyadic Green's functions $\mathbb{G}^{\mathrm{E}}(\mathbf{r},\mathbf{r}'',\omega)$ and $\mathbb{G}^{H}(\mathbf{r},\mathbf{r}'',\omega)$ for that layered geometry with

source points $\mathbf{r}''$ inside medium 1 and observation points $\mathbf{r}$ inside the vacuum gap. For the given layered geometry the Green's functions are well known and can for example be found in (Tsang et al. (2000)). For determining the net heat flux one has also to consider the opposite case with $T_1 = 0$ so that only fluctuating currents inside medium 2 are taken into account. Then the net heat flux inside the vacuum gap is given by the difference

$$\Phi = \langle S_z^{1\to 2}\rangle - \langle S_z^{2\to 1}\rangle. \tag{9}$$

For two isotropic media we find (Polder and Van Hove (1971))

$$\Phi = \int_0^\infty \frac{\mathrm{d}\omega}{2\pi}\left[\Theta(\omega,T_1) - \Theta(\omega,T_2)\right] \sum_{j=\{\mathrm{s},\mathrm{p}\}} \int \frac{\mathrm{d}^2\boldsymbol{\kappa}}{(2\pi)^2}\, \mathcal{T}_j(\omega,\boldsymbol{\kappa};d) \tag{10}$$

The second integral of the energy transmission coefficient $\mathcal{T}_j(\omega,\boldsymbol{\kappa};d)$ is carried out over all transverse wave vectors $\boldsymbol{\kappa} = (k_x,k_y)^{\mathrm{t}}$. This means it includes propagating modes as well as evanescent modes. The division into propagating and evanescent modes stems from the fact that the electromagnetic waves inside the vacuum gap region have a phase factor $\exp[\mathrm{i}(k_x x + k_y y + k_{z0} z) - \mathrm{i}\omega t]$ with $k_{z0} = \sqrt{\omega^2/c^2 - \kappa^2}$, where c is the velocity of light in vacuum. Hence, k_{z0} is purely real for all lateral wave vectors $\kappa < \omega/c$ and therefore the phase factor gives an oscillatory solution with respect to z, whereas k_{z0} is for all $\kappa > \omega/c$ purely imaginary so that the phase factor gives an exponential damping with respect to z. The latter modes are called evanescent modes, whereas modes with $\kappa < \omega/c$ are called propagating modes. Note, that the vacuum part in $\Theta(\omega,T)$ does not contribute to the flux Φ.

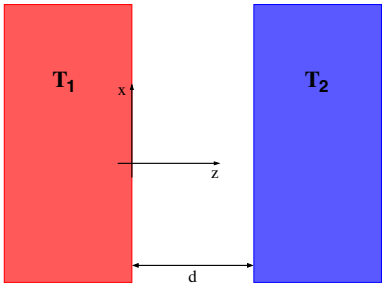

Fig. 1. Sketch of the considered geometry: Two semi-infinite materials at local thermal equilibrium with temperatures T_1 and T_2 are separated by a vacuum gap of thickness d.

The energy transmission coefficient $\mathcal{T}_j(\omega,\boldsymbol{\kappa};d)$ is different for propagating and evanescent modes and can be stated as (Polder and Van Hove (1971))

$$\mathcal{T}_j(\omega,\kappa;d) = \begin{cases} (1-|r_j^1|^2)(1-|r_j^2|^2)/|D_j^{12}|^2, & \kappa < \omega/c \\ 4\mathrm{Im}(r_j^1)\mathrm{Im}(r_j^2)\mathrm{e}^{-2|k_{z0}|d}/|D_j^{12}|^2, & \kappa > \omega/c \end{cases} \tag{11}$$

for $j = \{\mathrm{s},\mathrm{p}\}$ where r_j^1 and r_j^2 are the usual Fresnel coefficients

$$r_{\mathrm{s}}^i(\omega,\kappa) = \frac{k_{z0} - k_{zi}}{k_{z0} + k_{zi}} \qquad \text{und} \qquad r_{\mathrm{p}}^i(\omega,\kappa) = \frac{\epsilon_i(\omega)k_{z0} - k_{zi}}{\epsilon_i(\omega)k_{z0} + k_{zi}} \tag{12}$$

for s- and p-polarized light, where $k_{zi} = \sqrt{\epsilon_i(\omega)\omega^2/c^2 - \kappa^2}$. We have further introduced the Fabry-Pérot-like denominator D_j^{12}, defined by ($j = \{\mathrm{s}, \mathrm{p}\}$)

$$D_j^{12} = (1 - r_j^1 r_j^2 \mathrm{e}^{2\mathrm{i}k_{z0}d})^{-1} \tag{13}$$

which appears as a consequence of the multiple reflections inside the vacuum gap.

1.3 Nanoscale heat flux

The expression in Eq. (10) together with the energy transmission coefficient in Eq. (11) is very general and allows the determination of the heat flux between two arbitrary isotropic semi-infinite bodies kept at fixed temperatures T_1 and T_2 for any distance d. In particular this expression contains the Stefan-Boltzmann law for the heat flux between two *black bodies*. This can be seen as follows: a *black body* is a body which absorbs all incoming radiation. For a semi-infinite body this situation is realized, when the Fresnel reflection coefficients are exactly zero for both polarizations. Then all incoming radiation is transmitted and will be absorbed inside the semi-infinite medium. Hence, by assuming that the Fresnel coefficients are zero we obtain from Eq. (11) that the energy transmission coefficient $\mathcal{T}_j(\omega, \boldsymbol{\kappa}; d) = 1$ for s- and one for p-polarized light with $\kappa < \omega/c$ and $\mathcal{T}_j(\omega, \boldsymbol{\kappa}; d) = 0$ for $\kappa > \omega/c$. In other words, all propagating modes contribute with a maximal transmission of 1 to the heat flux. Then one can easily compute the heat flux from Eq. (10) yielding

$$\Phi_{\mathrm{BB}} = \int_0^\infty \left[\Theta(\omega, T_1) - \Theta(\omega, T_2)\right] \left(\frac{\omega^2}{c^3\pi^2}\right) \frac{c}{4} = \sigma_{\mathrm{BB}}(T_1^4 - T_2^4) \tag{14}$$

which is the well-known Stefan-Boltzmann law for the heat flux between two black bodies with the Stefan-Boltzmann constant $\sigma_{\mathrm{BB}} = 5.67 \cdot 10^{-8}\,\mathrm{Wm^{-2}K^{-4}}$.

From this derivation of the Stefan-Boltzmann law we see that it can be a limit for the propagating modes only, since only for these modes ($\kappa < \omega/c$) on the left of the light line $\omega = c\kappa$ [see Fig. 2 (a)] the energy transmission coefficient has its maximum value and is zero for the evanescent modes ($\kappa > \omega/c$) on the right of the light line in Fig. 2 (a). This fact can also be formulated in terms of the number of contributing modes. To this end consider a quantisation box in x and y direction with a length $L_x = L_y = L$. For very large L the integral over the lateral wave vectors in Eq. (10) is equivalent to a sum over the modes $k_x = 2\pi n_x/L$ and $k_y = 2\pi n_y/L$ with $n_x, n_y \in \mathbb{N}$, i.e.,

$$\int \frac{\mathrm{d}^2\kappa}{(2\pi)^2} = \frac{1}{L^2} \int \frac{\mathrm{d}^2\kappa}{\left(\frac{2\pi}{L}\right)^2} \leftrightarrow \frac{1}{L^2} \sum_{n_x, n_y} 1. \tag{15}$$

Here $\sum_{n_x,n_y} 1$ is the number of contributing modes and $L^{-2}\sum_{n_x,n_y} 1$ the density of states. Hence, for a given frequency ω only the modes in a circle [see Fig. 2 (b)] with radius ω/c contribute, but with a transmission factor of one for each polarisation, this means the number of contributing modes is limited to the region $\kappa < \omega/c$.

For real materials, the number of contributing modes is not limited to the region $\kappa < \omega/c$. As was already put forward by (Cravalho et al., (1967)) total internal reflection modes become frustrated if the gap distance d is much smaller than the thermal wavelength $\lambda_{\mathrm{th}} = \hbar c/(k_{\mathrm{B}}T)$ and can therefore tunnel through the vacuum gap and hence contribute to the heat flux. Since

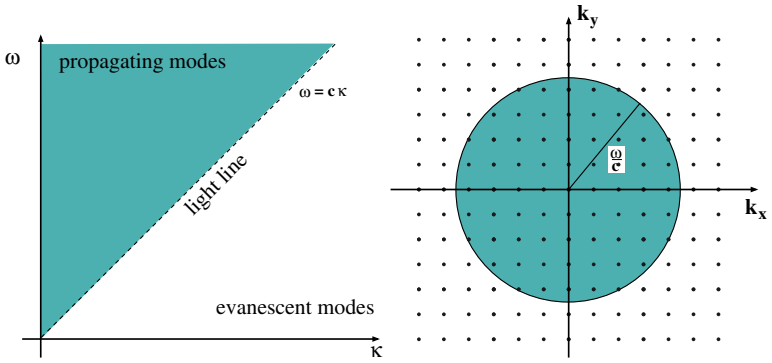

(a) ω-κ diagram (b) wave vector space

Fig. 2. Sketch of the contributing modes. (a) shows the ω-κ diagram. The light line at $\omega = c\kappa$ divides the ω-κ space into the propagating and evanescent part, i.e., the propagating modes inside the vacuum gap are on the left of the light line, whereas the evanescent modes are on the right of the light line. For a *black body* all propagating modes contribute with transmission 1 to the heat flux. (b) shows the space of lateral wave vectors for a fixed frequency ω. All modes inside the circle with radius ω/c are propagating modes, and all modes outside that circle are evanescent.

these modes are propagating inside the material but evanescent in the vacuum region they are determined by $\kappa > \omega/c$ and $\kappa < \sqrt{\epsilon_i(\omega)}\omega/c$. For a polar material as SiC, which can be described by the permittivity

$$\epsilon_1(\omega) = \epsilon_2(\omega) = \epsilon_\infty \left(\frac{\omega_L^2 - \omega^2 - i\gamma\omega}{\omega_T^2 - \omega^2 - i\gamma\omega} \right) \equiv \epsilon(\omega), \tag{16}$$

with the longitudinal phonon frequency $\omega_L = 1.827 \cdot 10^{14}\,\mathrm{rad/s}$, the transversal phonon frequency $\omega_T = 1.495 \cdot 10^{14}\,\mathrm{rad/s}$, the damping $\gamma = 0.9 \cdot 10^{12}\,\mathrm{rad/s}$ and $\epsilon_\infty = 6.7$, we illustrate schematically in Fig. 3 the regions for which one can expect frustrated modes. For the sake of simplicity we neglect the damping for the discussion of the contributing modes and assume a real permittivity. We will later add the absorption again, since it is vital for the nanoscale heat transfer. Note in Fig. 3(a), that in the so called *reststrahlen region* $\omega_T < \omega < \omega_L$ no optical phonons can be excited. Within this frequency band the permittivity is negative so that the material behaves effectively like a metal, i.e., the reflectivity is close to one. From Fig. 3 (b) it is obvious that due to the frustrated internal reflection the number of contributing modes for the heat flux increases, but is still limited to $\kappa < \sqrt{\epsilon(\omega)}\omega/c$.

Before we can discuss the energy transmission coefficient and the heat flux, we need to discuss another kind of evanescent mode which is responsible for the tremendous increase of the heat flux at nanoscale, the so-called surface phonon polariton (Kliewer and Fuchs (1974)). This mode is characterized by the fact that the electromagnetic fields are evanescent inside and outside the medium so that these modes are confined to the boundary of the medium itself. Assuming an infinite large distance d between the halfspaces, then both can be considered as individual semi-infinite bodies with negligible coupling. For such isotropic nonmagnetic halfspaces the surface modes are purely p-polarized and fulfill the dispersion

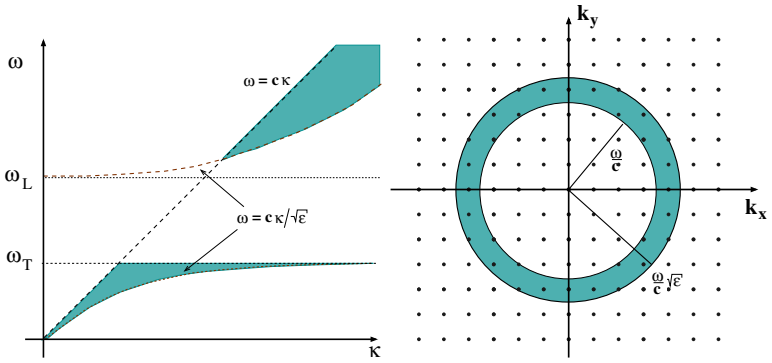

(a) ω-κ diagram (b) wave vector space

Fig. 3. Sketch of the frustrated modes. The modes which can propagate inside the dielectric are on the left of the polariton lines $\omega = c\kappa/\sqrt{\epsilon}$. The internal reflection modes are on the left of the polariton lines and on the right of the light line within the green region.

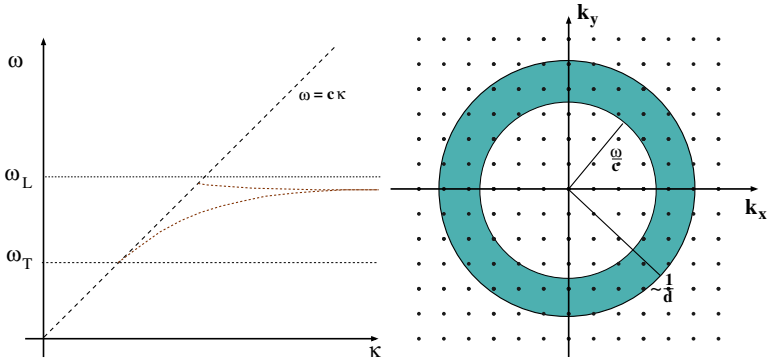

(a) ω-κ diagram (b) wave vector space

Fig. 4. Sketch of the surface phonon polariton modes for a given distance d.

relation (Kliewer and Fuchs (1974))

$$\kappa_{\mathrm{SPhP}} = \sqrt{\frac{\epsilon(\omega)}{\epsilon(\omega)+1}}. \tag{17}$$

Furthermore, a necessary condition for having surface modes is that $\epsilon(\omega) < 0$, i.e., for polar materials like SiC separated by vacuum it can only exist within the reststrahlen band $\omega_{\mathrm{T}} < \omega < \omega_{\mathrm{L}}$. When the two semi-infinite material are placed at a distance d smaller than the penetration length of this surface mode in vacuum, i.e., $1/\mathrm{Im}(\sqrt{\omega^2/c^2 - \kappa^2_{\mathrm{SPhP}}})$, these modes will couple. This coupling removes the two-fold degeneracy and produces a splitting of the dispersion relation (Raether (1988)), which is determined by the relation

$$\left[-\mathrm{Im}(r_{\mathrm{p}})^2 + \mathrm{Re}(r_{\mathrm{p}})^2 + 2\mathrm{i}\mathrm{Im}(r_{\mathrm{p}})\mathrm{Re}(r_{\mathrm{p}})\right]\mathrm{e}^{-2\mathrm{Im}(k_{z0}d)} = 1 \tag{18}$$

and schematically illustrated in Fig. 4 (a). Since we are interested in the transmission coefficient of such modes, we now consider a permittivity with absorption, or $\gamma \neq 0$. For small absorption, more precise for $\mathrm{Im}(r_\mathrm{p}) \ll \mathrm{Re}(r_\mathrm{p})$, the dispersion relation for the coupled surface modes coincides with the resonance condition of the energy transmission coefficient (Pendry (1999))

$$\left[-\mathrm{Im}(r_\mathrm{p})^2 + \mathrm{Re}(r_\mathrm{p})^2\right] \mathrm{e}^{-2\mathrm{Im}(k_{z0}d)} = 1 \tag{19}$$

for which the evanescent part of the energy transmission coefficient in Eq. (11) has its maximal value of one, i.e., the energy transmission coefficient is one for the surface phonon polaritons as long as $\mathrm{Im}(r_\mathrm{p}) \ll \mathrm{Re}(r_\mathrm{p})$ is fullfilled. Nonetheless, for very large $\kappa \gg d^{-1} \gg \omega/c$ the energy transmission coefficient in Eq. (11) is damped exponentially due to the exponential $\exp(-2\mathrm{Im}(k_{z0})d) \approx \exp(-2\kappa d)$. Here, the exact damping of the energy transmission coefficient is determined by the losses of the material (Biehs et al. (2010)). Hence, the coupled surface phonon polariton provides for distances smaller than $d \ll c/(\omega\sqrt{\epsilon(\omega)})$ a number of modes proportional to d^{-2} as illustrated in Fig. 4(b) contributing to the heat flux which eventually results in a larger contribution than that of the frustrated internal reflection modes.

Now we are in a good starting position to discuss the energy transmission coefficient between two semi-infinite SiC plates assuming that $T_1 = 300\,\mathrm{K}$ and $T_2 = 0$ so that $\lambda_\mathrm{th} = 7.6\,\mu\mathrm{m}$. For this purpose we plot in Fig. 5 the energy transmission coefficient $\mathcal{T}_\mathrm{p}(\omega, \kappa; d)$ in ω-κ space for distances (a) $d = 5\,\mu\mathrm{m}$, (b) $d = 500\,\mathrm{nm}$ and (c) $d = 100\,\mathrm{nm}$. In Fig. 5 (a) we observe that for a relatively large distance the transmission coefficient is dominated by the propagating modes on the left of the light line and is maximal for the Fabry-Pérot modes inside the gap. Nonetheless, the surface phonon polariton modes already contribute inside the reststrahlen region. One can observe that in this region the surface phonon mode dispersion is continued on the left of the light line. This mode is evanescent inside the medium, but propagating in the vacuum gap so that it can be considered as a wave guide mode. As for surface phonon polaritons these guided modes do not contribute to the energy flux if there is no absorption, i.e., if $\mathrm{Im}(\epsilon) = 0$, whereas the Fabry-Pérot modes and the frustrated modes do contribute. For smaller distances we can see in Fig 5(b) that the surface modes and frustrated modes come into play. For even smaller distances the energy transmission coefficient equals one for all modes which can exist inside the bulk SiC (on the left of the phonon polariton lines) and for the surface modes [see Fig. 5 (c)], which will give the main contribution to the heat flux, since the number of contributing modes is very large [see Fig. 5 (d)].

The resulting spectral heat flux Φ_ω is now plotted in Fig. 6(a). It can be observed that for very small distances the spectrum becomes quasi monochromatic around the frequency of the surface mode resonance $\omega_\mathrm{SPhP} = 1.787 \cdot 10^{14}\,\mathrm{rad/s}$ which is defined by the pole of the denominator in Eq. (17), i.e., through the implicit relations $\mathrm{Re}[\epsilon(\omega_\mathrm{SPhP})] = -1$ and $\mathrm{Im}[\epsilon(\omega_\mathrm{SPhP})] \ll 1$. The distance dependence is shown in Fig. 6(b) where the flux Φ is normalized to the heat flux between two black bodies $\Phi_\mathrm{BB} = 459.27\,\mathrm{Wm}^{-2}$. The contributions are divided into the propagating, the frustrated, and the surface phonon polariton part. One can clearly see that the heat flux rises for distances smaller than the thermal wavelength $\lambda_\mathrm{th} = 7.6\,\mu\mathrm{m}$ due to the frustrated modes and exceeds the black body limit at $d \approx 3\,\mu\mathrm{m}$. For even smaller distances ($d < 100\,\mathrm{nm}$) the surface modes start to dominate the heat flux completely and give a characteristic $1/d^2$ dependence, since the number of contributing modes is for these modes proportional to $1/d^2$. Note, that on the nanoscale at a distance of $d = 10\,\mathrm{nm}$ the heat flux exceeds the black body limit by a factor of 1000! For some asymptotic

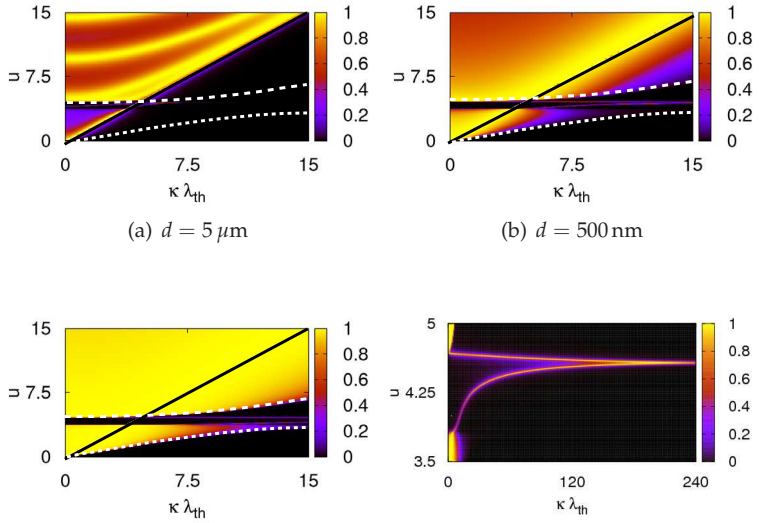

(a) $d = 5\,\mu\mathrm{m}$ (b) $d = 500\,\mathrm{nm}$

(c) $d = 100\,nm$ (d) $d = 100\,nm$

Fig. 5. Transmission coefficient $\mathcal{T}_\mathrm{p}(\omega, \kappa; d)$ between two SiC plates for different distances in ω-κ space. Note that (d) is the same as (c) but for a large κ range, showing that the number of contributing modes for the coupled surface modes is much larger than for the frustrated modes. The dashed lines are the phonon polariton lines for SiC. Here, $u = \hbar\omega/(k_\mathrm{B}T)$ is a rescaled frequency so that for $T = 300\,\mathrm{K}$ we have $\omega = u \cdot 4.14 \cdot 10^{13}\mathrm{rad/s}$.

expression concerning the heat flux in different distance regimes see (Rousseau et al. (2009b; 2010)).

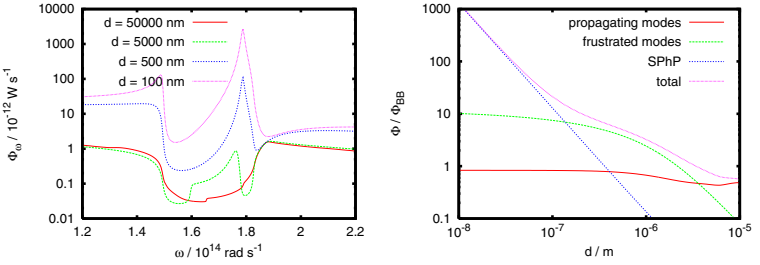

(a) spectral heat flux Φ_ω (b) total heat flux Φ

Fig. 6. (a) spectral heat flux Φ_ω between two SiC halfspaces at $T_1 = 300\,\mathrm{K}$ and $T_2 = 0\,\mathrm{K}$ for different distances. (b) total heat flux Φ over distance.

Finally, we want to express the formula for Φ in a way which highlights the number of modes contributing to the heat flux. To this end, we start with Eq. (10) assuming $T_1 = T$ and $T_2 = T + \Delta T$. For small temperature differences ΔT we can linearize Eq. (10) defining the radiative

heat transfer coefficient h_{rad} through

$$\Phi = h_{\mathrm{rad}}(T)\Delta T \equiv \frac{\partial \Phi}{\partial T}\Delta T. \tag{20}$$

By introducing the dimensionless variable $u = \hbar\omega/(k_{\mathrm{B}}T)$ and the mean transmission coefficient

$$\overline{\mathcal{T}}_j = \frac{\int_0^\infty \mathrm{d}u\, f(u)\mathcal{T}_j(u,\kappa;d)}{\int_0^\infty \mathrm{d}u\, f(u)} \tag{21}$$

with $f(u) = u^2\mathrm{e}^u/(\mathrm{e}^u-1)^2$ we find a Landauer-like expression for the heat flux (Biehs et al. (2010))

$$\Phi = \frac{\pi^2}{3}\frac{k_{\mathrm{B}}^2 T}{\mathrm{h}}\left(\sum_{j=\mathrm{s,p}}\int\frac{\mathrm{d}^2\kappa}{(2\pi)^2}\overline{\mathcal{T}}_j\right)\Delta T. \tag{22}$$

Here, $\pi^2 k_{\mathrm{B}}^2 T/(3\mathrm{h})$ is the universal quantum of thermal conductance (Pendry (1983); Rego and Kirczenow (1999)). Hence, each mode can at most contribute one quantum of thermal conductance, since the mean transmission coefficient $\overline{\mathcal{T}}_j \in [0,1]$. This representation allows for studying the tradeoff between the mean transmission coefficient and the number of modes. In Fig. 7 we show a plot of the mean transmission coefficient $\overline{\mathcal{T}}_{\mathrm{p}}$ for two SiC slabs varying the distance. It can be seen that the mean transmission coefficient for the surface modes is extremely small. Nonetheless, the coupled surface modes give the dominant heat transfer mechanism for small distances. This is due to the number of modes which increases dramatically $\propto \kappa^2$ explaining the $1/d^2$ increase in heat flux due to the coupled surface modes. For polar materials there is a cutoff value for the spatial wave vectors of the phonons given by π/a, where a is the lattice constant. This sets an ultimate limit to the heat flux and removes the $1/d^2$ divergency. The limits of the heat flux in the near-field regime are for example disscussed in Refs. (Basu and Zhang (2009); Ben-Abdallah and Joulain (2010)).

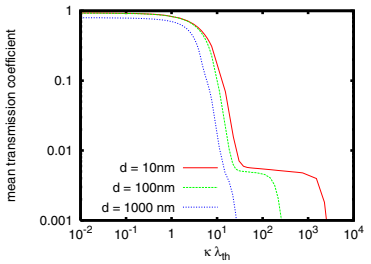

Fig. 7. Mean transmission coefficient $\overline{\mathcal{T}}_{\mathrm{p}}$ for two SiC slabs with varying distances d.

2. Thermal imaging

Measurement and control of temperature at the nanoscale are important issues in nanotechnology. There are nowadays several possibilities for mapping the temperature above a surface or a nanostructure. For instance, the fluorescence polarization anisotropy of suspended molecules placed around a nanostructure can be used to map the local temperature of nanoscaled sources (Baffou et al. (2009)). On the other hand, the properties of the fluctuating electromagnetic fields can directly be used for a contact-free measurement of surface properties as local temperatures and local material properties. One step in this

direction was done by De Wilde *et al.* (De Wilde et al. (2006)) [and recently Kajihara *et al.* (Kajihara et al. (2010))] who have developed a SNOM-based method in order to scatter the thermal near field into the far field and to measure the photonic local density of states of that surface. Very recently, a similar but promising imaging method was established which consist in measuring the thermal near-field spectra of surfaces in order to characterize their material properties as for instance the local free-carrier concentration and mobility (Huth et al. (2011)).

Here, we will review a method of thermal imaging called near-field scanning thermal microscopy (NSThM), which was developed in the Oldenburg group of Achim Kittel and Jürgen Parisi (Kittel et al (2005); Müller-Hirsch et al. (1999); Wischnath et al (2008)). It is based on an STM tip which is augmented by a thermocouple in the tip apex. With the help of the STM ability one can control the surface-tip distance, whereas the thermocouple allows for measuring the local temperature at the tip position, which can be varied in a distance range of 0.1 nm to about 100 nm. In contrast to usual thermal profilers used in scanning thermal microscopy (SThM), the NSThM probe operates at ultra high vacuum conditions rather than at ambient conditions (Majumdar (1999)). Hence, the energy or heat flow is not mediated by gas molecules, nor a liquid film of adsorbates, nor solid-solid conduction, but by the near field interaction between the tip and the sample mediated by the fluctating electromagnetic field. In other words, the NSThM exploits the enhanced radiative heat transfer at the nanoscale for surface imaging.

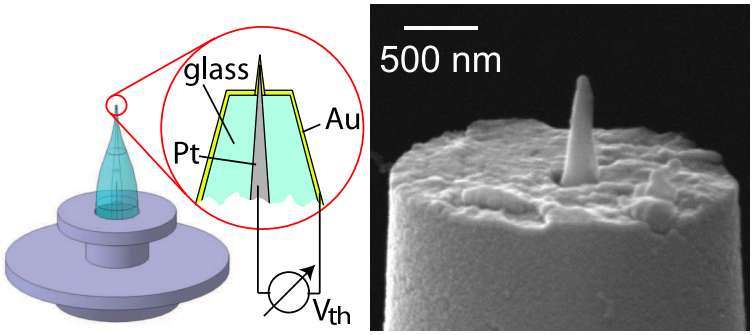

(a) Schematic drawing of the NSTHM (b) SEM image of a typical NSTHM tip. tip.

Fig. 8. Near field scanning thermal microscope developed in the group of Achim Kittel in Oldenburg (Kittel et al. (2008)). Reprinted with permission from Appl. Phys. Lett., Vol. **93**, 193109 (2008). Copyright 2008, American Institute of Physics.

As shown in Fig. 8 the tip consists of a platinum wire protruding about 500 nm from a glass capillary. A gold coating establishes the gold-platinum thermocouple in coaxial configuration at the very end of the tip. At the foremost part the tip radius is less than 50 nm allowing for a high lateral resolution when scanning a sample surface. When the probe is moving in proximity to a cold or hot sample surface the tip is slightly cooled down or heated up at the very end resulting in a temperature gradient within the tip. This temperature gradient is the source of a thermovoltage V_{th} which is the measured quantity. Now, the thermovoltage is directly proportional to the temperature difference ΔT_{tip} in the tip wich allows for determining the local temperature of the sample surface or the heat flow between the tip and the sample.

In particular, for the heat flux Φ one has (Wischnath et al (2008))

$$\Phi = V_{\rm th} \frac{1}{S R_{\rm th}^{\rm pr}} \tag{23}$$

where S is the Seebeck coefficient of the probe's thermocouple and $R_{\rm th}^{\rm pr}$ is its thermal resistance, which can in principle be determined experimentally. Hence, the heat flow is also directly proportional to $V_{\rm th}$ times a tip-dependent factor of proportionality.

In order to provide an interpretation of the data measured with an NSThM tip one can model it as a simple dipole associated with a given temperature T_1 situated at $\mathbf{r}_{\rm tip}$ above the sample surface with a temperature T_2 as sketched in Fig. 9. Within such a simple dipole model it can be shown that the heat flux is given by (Chapuis et al. (2008b); Dedkov and Kyasov (2007); Dorofeyev (1998); Mulet et al. (2001); Pendry (1999))

$$\Phi = \sum_{i={\rm E,M}} \int_0^\infty {\rm d}\omega \, 2\omega {\rm Im}[\alpha_i(\omega)] \left[\Theta(\omega, T_1) - \Theta(\omega, T_2)\right] D^i(\omega, \mathbf{r}_{\rm tip}) \tag{24}$$

where $\alpha_{\rm E/M}$ is the electric/magnetic polarizability of the tip apex and $D^{\rm E/M}(\omega, \mathbf{r}_{\rm tip})$ is the electric/magnetic local densitiy of states (LDOS) above the sample surface (Joulain et al. (2003)). Here, the spectral power absorbed by the tip apex is given by ${\rm Im}[\alpha_i(\omega)] D^i(\omega, \mathbf{r}_{\rm tip}) \Theta(\omega, T_2)$, i.e., it is proportional to the imaginary part of the polarizability of the tip and proportional to the energy density above the surface which is given by the product $D^i(\omega, \mathbf{r}_{\rm tip}) \Theta(\omega, T_2)$. On the other hand the power emitted by the tip and absorbed within the bulk medium is proportional to ${\rm Im}[\alpha_i(\omega)] D^i(\omega, \mathbf{r}_{\rm tip}) \Theta(\omega, T_1)$. In fact, when considering the flux between two metals not supporting surface plasmons for $T_1 = 300\,{\rm K}$ and $T_2 \ll T_1$ this expression simplifies to (Biehs et al. (2008); Rüting et al. (2010))

$$\Phi \propto {\rm Im}[\alpha_M(\omega_{\rm th})] D^M(\omega_{\rm th}, \mathbf{r}_{\rm tip}). \tag{25}$$

This means, the heat flux is directly proportional to the magnetic LDOS above the sample evaluated at the tip position $\mathbf{r}_{\rm tip}$ and the thermal frequency $\omega_{\rm th} \approx 2.82 k_{\rm B} T/\hbar$. Hence, roughly speaking by measuring the thermovoltage the NSThM measures the LDOS of the sample surface. Note, that this expression is strictly valid for surface tip distances much larger than the tip radius only assuming a spherical metallic sensor tip. Indeed the value of the heat flux as well as the thermal near-field image of a structured surface depend on the shape and the material properties of the tip apex as was shown for ellipsoidal sensor tips (dielectric and metallic) in (Biehs et al. (2010b); Huth et al. (2010)). Hence, for a more refined model it is important to account for the sensor shape and to include the contributions of higher multipoles.

For structured as well as for rough surfaces (Biehs et al. (2010c;d; 2008); Rüting et al. (2010)) the LDOS can be calculated pertubatively by using for example the perturbation approach of (Greffet (1988)) if the height differences of the surface profile are the smallest length scales and in particular smaller than the thermal wavelength (Henkel and Sandoghdar (1998)). This allows for comparision of the NSThM data with theory, i.e., with the numerically evaluated LDOS $D^M(\omega_{\rm th}, \mathbf{r}_{\rm tip})$. To this end, one can use the STM ability of the NSThM probe to obtain the topographical information of the sample surface. Using this data for the theoretical calculation one can compare the theoretical results for the LDOS with the measured thermovoltage $V_{\rm th}$.

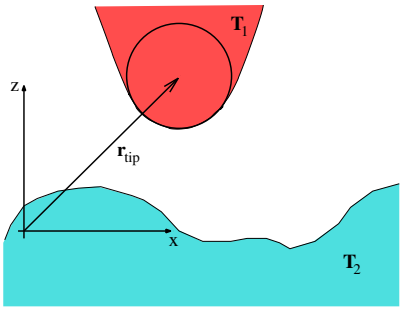

Fig. 9. Schematic of the tip-sample geometry. The sensor tip is assumed to have a spherical tip apex so that it can be modeled by a simple dipole placed in the center of the tip apex at $\mathbf{r}_{\mathrm{tip}}$.

Such a comparision is shown in Fig. 10 for the scan of a 100 nm $\times$ 100 nm gold surface. During the measurement the gold surface is cooled down to about 110 K, whereas the tip is kept at 293 K. The tip-surface distance is kept constant and is smaller than 1 nm. Due to this small distance the dipole model together with the first-order perturbation theory is strictly speaking not valid anymore. Nonetheless, the data fit very well with the LDOS calculated for a constant distance of 9 nm above the surface showing that the measured signal follows qualitatively the LDOS of the thermal electromagnetic field above the surface profile evaluated at the dominant thermal frequency $\omega_{\mathrm{th}} \approx 10^{14}\,\mathrm{rad/s}$. Further quantitative comparisions with the predictions of a refined model for different samples and scan modi are desirable for exploring the possibilities opened up by the NSThM.

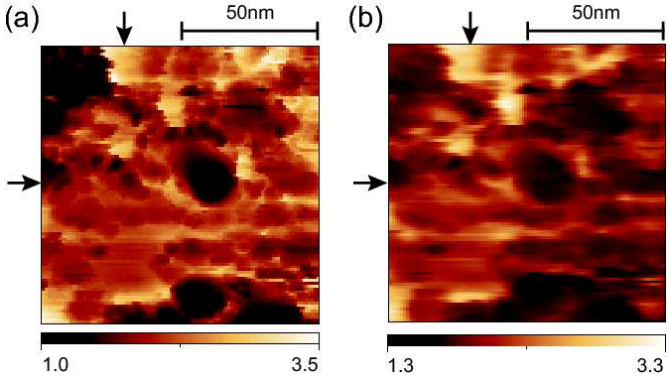

Fig. 10. (a) Numerically calculated LDOS in $10^6\ \mathrm{m}^{-3}\,\mathrm{s}$ at a constant distance of 9 nm above the two-dimensional topography directly extracted from the STM data (b) A plot of the thermovoltage data which corresponds to the temperature gradient in the tip and varies as the temperature in the tip apex varies (in arbitrary units). Reprinted with permission from Appl. Phys. Lett., Vol. **93**, 193109 (2008). Copyright 2008, American Institute of Physics.

In summary, the NSThM provides the possibility for a contact-free measurement of surface properties by exploiting the enhanced radiative heat flux at the nanoscale. In particular, it allows for measuring the heat flux between the nanometer-sized tip and a surface in a distance regime of a few nanometers above the sample surface. The measured thermovoltage signal

is not only proportional to the heat flux between the tip and the sample surface, but also facilitates the measurement of the local surface temperature. On the other hand, since the heat flux depends on the material properties of the sample, the measured signal could also be used to access local material properties, while a spectral measurement as in (Huth et al. (2011)) is more suitable for that purpose.

3. Thermal management with anisotropic media

A proper understanding of near-field heat transfer naturally gave rise to new ideas on how to control the heat flux between closely separated structures, i.e., on *thermal management* at the micro/nanoscale. Such a control can be achieved, for instance, by thermal rectifiers (Basu and Francoeur (2011); Otey et al (2010)), thermal transistors (Ojanen and Jauho (2008)) and thermal modulators (Biehs et al. (2011b); van Zwol et al (2010)) for thermal photons. Here we review a very interesting approach to heat-flux modulation that consists in actively changing the relative orientation of electrically anisotropic materials, while keeping a fixed (small) distance between them. However, before going into the specifics of that subject we would like to briefly comment another approach to heat flux modulation, namely, with the use of phase change materials.

In our context, a phase change material (PCM) can be defined as a medium that shows two distinct solid phases, one amorphous and the other crystalline, and that can be switched from one to the other in a sufficiently short time (Wuttig and Yamada (2007)). The switching typically goes through the liquid phase as well, and can be summarized in a series of three steps (Wuttig and Yamada (2007)). First we take a PCM in the crystalline phase and heat it up quickly with an intense short pulse. The subsequent cooling is thus also very fast and leads to a quenching process, trapping the material in an amorphous state. The return to the crystalline state is performed by a weaker and longer pulse, that heats up the medium just enough to allow the transition. The considerable difference in optical and electrical properties between the amorphous and crystalline states of some PCMs opens the door to several potentially interesting applications. Among them, we find the possibility of actively controlling the heat flux by switching the PCM back and forth among its two phases, which can be done as fast as 100 ns (Wuttig and Yamada (2007)). Not only the modulation is quick, but it was also shown (van Zwol et al (2010; 2011b)) that for certain distances the switching changes the heat flux by one order of magnitude and that the cycle is fairly repeatable ($10^7 - 10^{12}$ times), making it a good candidate for possible applications in thermal management.

3.1 The heat transfer between planar anisotropic materials

In order to fix ideas, let us consider the situation depicted in Fig. 1,where we have two linear semi-infinite media at different temperatures, but at this point not necessarily homogeneous or isotropic. The expression for the transfered heat is given by

$$\mathrm{H_F}(T_1, T_2, a) = \int_A \mathbf{dA} \cdot \langle \mathbf{S}^{1\to 2} - \mathbf{S}^{2\to 1} \rangle = \int_{z=0} \mathrm{d}^2\mathbf{r}_{\|} \langle S_z^{1\to 2} - S_z^{2\to 1} \rangle, \tag{26}$$

where $\mathbf{r}_{\|} = (x, y)$ and $S_z^{1\to 2}$ is given by (8) and the integration can be over any surface A that completely separates the bodies, that for convenience (and with no loss of generality) we took as the plane $z = z_0$. By using the Fourier expansions (3) and the Green's dyad introduced in

(4, 5), we can recast the integrand of the previous expression into

$$\langle S_z \rangle = \int_0^\infty \frac{\mathrm{d}\omega}{2\pi} \left[\Theta(\omega, T_1) - \Theta(\omega, T_2)\right] \langle S_\omega \rangle, \tag{27}$$

where (Volokitin and Persson (2007))

$$\langle S_\omega \rangle = 2\,\mathrm{Re}\,\mathrm{Tr} \int \mathrm{d}\mathbf{r}'_\parallel \left(\mathbb{G}(\mathbf{r}, \mathbf{r}') \partial_z \partial'_z \mathbb{G}^\dagger(\mathbf{r}, \mathbf{r}') - \partial_z \mathbb{G}^\dagger(\mathbf{r}, \mathbf{r}') \partial'_z \mathbb{G}(\mathbf{r}, \mathbf{r}') \right) \Big|_{z'=z=z_0}. \tag{28}$$

and $\Theta(\omega, T_i)$ was defined in (10).

The conclusion that we draw from Eqs. (26)-(28) is that, in order to evaluate the heat transfer for a given geometry we have to determine the Green's dyadic inside the gap region. In most cases this is surely a formidable task, but for planar homogeneous media, even if anisotropic, it is possible to simplify things enough so semi-analytic expressions are obtainable. This is not to say that everything was made easy - in fact even in this simplified case the calculations are fairly long (Chew (1995); Tomaš (2002)) [or requires some indirect arguments, see (Philbin and Leonhardt (2008))], so we shall just quote the final result for the Green tensor

$$\begin{aligned} \mathbb{G}(\mathbf{r}, \mathbf{r}') \; &= \frac{\mathrm{i}}{2} \int \mathrm{d}^2\boldsymbol{\kappa} \, \frac{e^{i\boldsymbol{\kappa}\cdot(\mathbf{r}_\parallel - \mathbf{r}'_\parallel)}}{k_{z0}} \Big[\mathbb{D}_{12} \Big(\mathbb{1} \mathrm{e}^{\mathrm{i}k_{z0}(z-z')} + \mathbb{R}_1 \mathrm{e}^{\mathrm{i}k_{z0}(z+z')} \Big) \\ &+ \mathbb{D}_{21} \Big(\mathbb{R}_2 \mathbb{R}_1 \mathrm{e}^{\mathrm{i}k_{z0}(z'-z)} \mathrm{e}^{2\mathrm{i}k_{z0}d} + \mathbb{R}_2 \mathrm{e}^{2\mathrm{i}k_{z0}d} \mathrm{e}^{-\mathrm{i}k_{z0}(z+z')} \Big) \Big], \end{aligned} \tag{29}$$

where $\mathbb{R}_i$ $(i = 1, 2)$ are the 2×2 reflection matrices characterizing interfaces (to be extensively discussed in the next section) and $\mathbb{D}_{ij}$ are defined by

$$\mathbb{D}_{ij} = (\mathbb{1} - \mathbb{R}_i \mathbb{R}_j \mathrm{e}^{2\mathrm{i}k_{z0}d})^{-1}. \tag{30}$$

When inserting Eq. (29) into the heat flux formula we find the analogue of (10) for anisotropic media, which reads (Biehs et al. (2011))

$$\langle S_\omega \rangle = \int \frac{\mathrm{d}^2\boldsymbol{\kappa}}{(2\pi)^2} \, \mathcal{T}_\mathrm{A}(\omega, \boldsymbol{\kappa}, d), \tag{31}$$

where

$$\mathcal{T}_\mathrm{A}(\omega, \boldsymbol{\kappa}, d) = \begin{cases} \mathrm{Tr}\left[(\mathbb{1} - \mathbb{R}_2^\dagger \mathbb{R}_2) \mathbb{D}_{12} (\mathbb{1} - \mathbb{R}_1^\dagger \mathbb{R}_1) \mathbb{D}_{12}{}^\dagger\right], & \kappa < \omega/c \\ \mathrm{Tr}\left[(\mathbb{R}_2^\dagger - \mathbb{R}_2) \mathbb{D}_{12} (\mathbb{R}_1 - \mathbb{R}_1^\dagger) \mathbb{D}_{12}{}^\dagger\right] \mathrm{e}^{-2|k_{z0}|d}, & \kappa > \omega/c \end{cases} \tag{32}$$

where Tr stands for the two-dimensional trace. From the previous equation we see that the whole problem is now reduced essentially to the calculation of the reflection matrices $\mathbb{R}_1, \mathbb{R}_2$, meaning that the problem has become essentially classical: the reflection coefficients can be found by considering a classical plane wave impinging on a vacuum/magnetodielectric interface, with no fluctuating fields involved. Since this is a somewhat long exercise, we give an outline for it in the next section.

3.2 Reflection coefficients for anisotropic materials

Let us consider the situation depicted on Fig. 11, that shows an incoming plane wave being reflected by an anisotropic (homogeneous) half-space. In the orthonormal coordinate system defined by the incident plane the incident fields are

$$\mathbf{E}_{\text{in}} = \left[e^{\text{s}}_{\text{in}} \hat{\mathbf{y}}' + e^{\text{p}}_{\text{in}} \frac{c}{\omega} (q_{\text{in}} \hat{\mathbf{x}}' - k_{x'} \hat{\mathbf{z}}') \right] e^{i(k_{x'} x' + q_{\text{in}} z' - \omega t)}, \tag{33}$$

$$\mathbf{H}_{\text{in}} = \left[e^{\text{p}}_{\text{in}} \hat{\mathbf{y}}' - e^{\text{s}}_{\text{in}} \frac{c}{\omega} (q_{\text{in}} \hat{\mathbf{x}}' - k_{x'} \hat{\mathbf{z}}') \right] e^{i(k_{x'} x' + q_{\text{in}} z' - \omega t)}, \tag{34}$$

where e^{s}_{in}, e^{p}_{in} are respectively the transverse electric (TE) and transverse magnetic (TM) incoming amplitudes, and we defined $k_{x'} = (\omega/c) \sin\theta_{\text{in}}$ and $q_{\text{in}} = (\omega/c) \cos\theta_{\text{in}}$. The reflected wave has a similar expression

$$\mathbf{E}_{\text{ref}} = \left[e^{\text{s}}_{\text{ref}} \hat{\mathbf{y}}' - e^{\text{p}}_{\text{ref}} \frac{c}{\omega} (q_{\text{in}} \hat{\mathbf{x}}' + k_{x'} \hat{\mathbf{z}}') \right] e^{i(k_{x'} x' - q_{\text{in}} z' - \omega t)}, \tag{35}$$

$$\mathbf{H}_{\text{ref}} = \left[e^{\text{p}}_{\text{ref}} \hat{\mathbf{y}}' + e^{\text{s}}_{\text{ref}} \frac{c}{\omega} (q_{\text{in}} \hat{\mathbf{x}}' + k_{x'} \hat{\mathbf{z}}') \right] e^{i(k_{x'} x' - q_{\text{in}} z' - \omega t)}, \tag{36}$$

where we have used $q_{\text{ref}} = -q_{\text{in}}$. Our problem now consists in finding the amplitudes $e^{\text{s}}_{\text{ref}}$, $e^{\text{p}}_{\text{ref}}$, so we can construct the reflection matrix given by

$$\mathbb{R}_j = \begin{bmatrix} r_j^{\text{s,s}}(\omega, \boldsymbol{\kappa}) & r_j^{\text{s,p}}(\omega, \boldsymbol{\kappa}) \\ r_j^{\text{p,s}}(\omega, \boldsymbol{\kappa}) & r_j^{\text{p,p}}(\omega, \boldsymbol{\kappa}) \end{bmatrix}, \tag{37}$$

where, by definition

$$\begin{aligned} r_j^{\text{s,s}}(\omega, \boldsymbol{\kappa}) &= \frac{e^{\text{s}}_{\text{ref}}}{e^{\text{s}}_{\text{in}}} \quad , \quad r_j^{\text{p,s}}(\omega, \boldsymbol{\kappa}) = \frac{e^{\text{p}}_{\text{ref}}}{e^{\text{s}}_{\text{in}}} \\ r_j^{\text{s,p}}(\omega, \boldsymbol{\kappa}) &= \frac{e^{\text{s}}_{\text{ref}}}{e^{\text{p}}_{\text{in}}} \quad , \quad r_j^{\text{p,p}}(\omega, \boldsymbol{\kappa}) = \frac{e^{\text{p}}_{\text{ref}}}{e^{\text{p}}_{\text{in}}} \end{aligned} \tag{38}$$

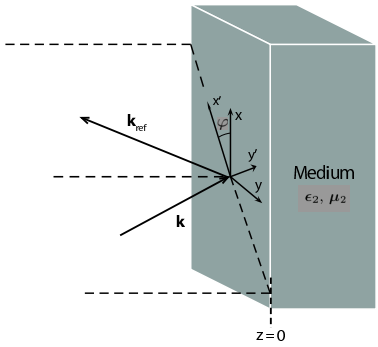

Fig. 11. An incident plane wave impinging on an anisotropic material.

The determination of such amplitudes is carried out by solving Maxwell's equations and imposing the proper boundary conditions on the interface (and on infinity). That means that

we have to find the transmitted amplitudes as well, which in turn requires that we state the constitutive relations for the materials involved. For anisotropic magnetodielectric media we have

$$\mathbf{D} = \boldsymbol{\epsilon} \cdot \mathbf{E} = \begin{bmatrix} \epsilon_{xx} & \epsilon_{xy} & \epsilon_{xz} \\ \epsilon_{yx} & \epsilon_{yy} & \epsilon_{yz} \\ \epsilon_{zx} & \epsilon_{zy} & \epsilon_{zz} \end{bmatrix} \cdot \begin{bmatrix} E_x \\ E_y \\ E_z \end{bmatrix} \quad \text{and} \quad \mathbf{B} = \boldsymbol{\mu} \cdot \mathbf{H} = \begin{bmatrix} \mu_{xx} & \mu_{xy} & \mu_{xz} \\ \mu_{yx} & \mu_{yy} & \mu_{yz} \\ \mu_{zx} & \mu_{zy} & \mu_{zz} \end{bmatrix} \cdot \begin{bmatrix} H_x \\ H_y \\ H_z \end{bmatrix} \tag{39}$$

where it is assumed that (i) the material tensors $\boldsymbol{\epsilon}$ and $\boldsymbol{\mu}$ are functions of frequency only, so no spatial dispersion is present, and that (ii) the materials involved do not present what is called bi-anisotropy (Tsang et al. (2000)), which manifests itself in non-vanishing cross couplings between **D** and **H** (and also **B** and **E**), and finally that (iii) the whole system is time-reversible, implying on $\epsilon_{xy} = \epsilon_{yx}$, $\mu_{xy} = \mu_{yx}$ (Landau and Lifshitz (2007)).

The degree of anisotropy of a material is roughly governed by the eigenvalues and eigenvectors of $\boldsymbol{\epsilon}$ and $\boldsymbol{\mu}$, which are in turn connected to the crystallographic structure of the material (Landau and Lifshitz (2007)). In the simplest case we have a cubic lattice, which has completely degenerate eigenvalues and is therefore not different from an isotropic medium. In the next level we have the trigonal, tetragonal and hexagonal lattices (Kittel (1962)), all characterized by two degenerate eigenvalues, or, in other words, by a preferred axis. Increasing the complexity a bit more we get to the orthorhombic lattice (Kittel (1962)), which presents 3 different eigenvalues but still has the eigenvectors crystallographic fixed (and orthogonal to each other). Finally, in the top of the list are the monoclinic and triclinic lattices (Kittel (1962)), which have no eigenvalue degeneracy and show also the so-called dispersion of axes (Landau and Lifshitz (2007)), meaning that the direction of the eigenvectors depend upon frequency.

Substituting the constitutive relations into Maxwell's equations (1)-(2), we get

$$\nabla \cdot (\boldsymbol{\epsilon} \cdot \mathbf{E}) = 0 \,, \qquad \nabla \cdot \mathbf{B} = 0 \tag{40}$$

$$\nabla \times \mathbf{E} = -\frac{1}{c} \frac{\partial \mathbf{B}}{\partial t} \,, \qquad \nabla \times (\boldsymbol{\mu}^{-1} \cdot \mathbf{B}) = \frac{1}{c} \boldsymbol{\epsilon} \cdot \frac{\partial \mathbf{E}}{\partial t}, \tag{41}$$

again reminding that we are now solving a classical reflection/transmission problem, so $\rho(\mathbf{r}, t) = \mathbf{j}(\mathbf{r}, t) = 0$. By assuming plane waves as solutions inside the material as well, we get

$$\begin{aligned} \mathbf{E} &= \mathbf{e}(z') e^{i(k_{x'} x' - \omega t)} \,, \qquad \mathbf{e} = (e_{x'}, e_{y'}, e_{z'}), \\ \mathbf{H} &= \mathbf{h}(z') e^{i(k_{x'} x' - \omega t)} \,, \qquad \mathbf{h} = (h_{x'}, h_{y'}, h_{z'}), \end{aligned} \tag{42}$$

and using that k_x is conserved across the interface, we see that the z' components can be eliminated as

$$e_{z'} = -c k_{x'} h_{y'} / \omega \epsilon_{z'z'} \,, \qquad h_{z'} = c k_{x'} e_{y'} / \omega \mu_{z'z'}, \tag{43}$$

leaving a total of 4 linearly independent solutions for a given $k_{x'}$ and ω (Chew (1995)). In order to determine the remaining x' and y' components of **e** and **h** it is convenient to introduce

a vector $\mathbf{u}$ with components $u_1 = e_{x'}$, $u_2 = e_{y'}$, $u_3 = h_{x'}$ and $u_4 = h_{y'}$. With the ansatz $u_j = u_j(0)e^{iqz'}$ we can transform (40)-(41) into an algebraic linear system of equations

$$\mathbf{L} \cdot \mathbf{u} = -\frac{c}{\omega} q \, \mathbf{u}, \tag{44}$$

where $\mathbf{L}$ is a 4×4 matrix and the possible q's are determined by

$$\det\left(\mathbf{L} + \frac{\omega q}{c}\mathbf{I}\right) = 0. \tag{45}$$

The analytical solutions of (44) and (45) for an arbitrary anisotropic magnetoelectric behavior are certainly very cumbersome, and to best of our knowledge they were never written down explicitly. The general case for electric anisotropy only ($\mu_{ij} = \delta_{ij}$) was dealt in (Teitler et al (1970)), while the magnetoelectric orthorhombic case was treated in (Rosa et al. (2008)). Due to the size and scope of this work it is not possible to reproduce the details here, so the interested reader is kindly referred to the references just mentioned in order to find the explicit solutions not only to (44) and (45) but also to the reflection coefficients themselves.

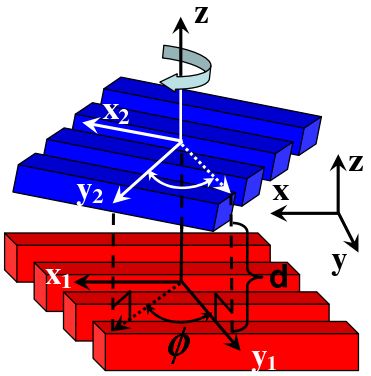

Fig. 12. Two gratings at different temperatures twisted with respect to each other. Reprinted with permission from Appl. Phys. Lett., Vol. **98**, 243102 (2011). Copyright 2008, American Institute of Physics.

3.3 Results

With the explicit expressions for the reflection matrices, we can calculate the transmission factor in (32) and therefore the heat transfer (27) with (31). In order to have a concrete situation in mind, let us imagine that we have the situation depicted in the Fig. 12, where two grating structures are facing each other at an arbitrary twisting angle (Biehs et al. (2011b)). In the effective medium approximation, those gratings may be described as anisotropic media with different dielectric/conduction properties in y and x, z directions. Assuming a simple Maxwell-Garnett model (Tao et al (1990)) for the respective permittivities, we get

$$\epsilon^i_{xx}(\omega) = \epsilon^i_{zz}(\omega) = \epsilon_{\mathrm{h}_i}(\omega)(1 - f_i) + f_i \quad , \quad \epsilon^i_{yy}(\omega) = \frac{\epsilon_{\mathrm{h}_i}(\omega)}{(1 - f_i) + f_i \epsilon_{\mathrm{h}_i}(\omega)}, \tag{46}$$

where ϵ_{h_i} is the permittivity of the i-th host medium, and f_i is the filling factor of the air inclusions in the i-th grating.

Substituting expressions (46) into (35)-(40) of Ref. (Rosa et al. (2008)) and then into (31) we get the heat transfer between the two gratings in the effective medium approximation. In Fig. 13(a) we plot the heat flux between two gold gratings as a function of the relative angle of twist between them, for fixed distances. We see that the flux is dramatically reduced as we twist the gratings, up to almost 80% at $\phi = \pi/2$ for distances as large as 1 μm. Unfortunately there is no simple physical picture that allows us to understand such effect, but it clearly indicates that symmetric configurations transmit heat more efficiently that asymmetric ones. This is further supported by Fig. 13(b), where the heat flux between two SiC gratings is shown. The reduction in the flux is less impressive in this case (although still quite significative), but the upside is that here we have more direct interpretation: for SiC gratings the surface modes give an important contribution to the flux, so it is intuitive that mismatching surface mode dispersion relations (for twisted structures) couple less effectively than matching ones (for parallel gratings) and will therefore give rise to a smaller transmission factor, and that is indeed what is observed.

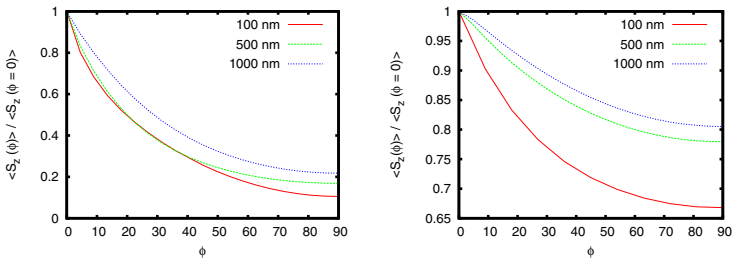

(a) Au (b) SiC

Fig. 13. The heat flux $\langle S_z \rangle(\phi)$ between two (a) Au and (b) SiC gratings, normalized by the flux $\langle S_z \rangle(0^\circ)$ when the gratings are aligned. The angle ϕ measures the relative twisting between the gratings, and the filling factor is fixed at $f = 0.3$. Reprinted with permission from Appl. Phys. Lett., Vol. **98**, 243102 (2011). Copyright 2008, American Institute of Physics.

Going back to the Au gratings, we see that the large suppression obtained by just rotating the structures with respect to one another suggests that such a setup could be used as a thermal modulator controlled by the twisting angle: in the parallel position there would be a heat flux (position "on"), in the orthogonal one there would not (position "off"). The on/off switching could as fast as several tens of kilohertz, and it would be extremely robust as the relative rotation does not wear off the material. Such thermal modulators can for example be interesting for fast heat flux modulation and thermal management of nano-electromechanical devices (Biehs et al. (2011b)).

4. Near-field thermophotovoltaics

Thermophotovoltaic (TPV) devices (Coutts (1999)) are energy conversion systems that generate electric power directly from thermal radiation. The basic principle (see Fig. 14) is similar to the classical photovoltaic conversion. A source of photons radiates in the direction of a p-n junction which converts the photons which have a sufficient energy into electron-hole pairs which, in turn, can be used to generate electricity. However contrary to classical systems, TPV devices operates in the near-infrared and not in the visible range. The efficiency of a photovoltaic cell is defined as the ratio $\eta = P_{\rm el}/P_{\rm rad}$ of the electric power $P_{\rm el}$ produced by the

photovoltaic cell and the net radiative power P_{rad} exchanged between the hot source and the p-n junction.

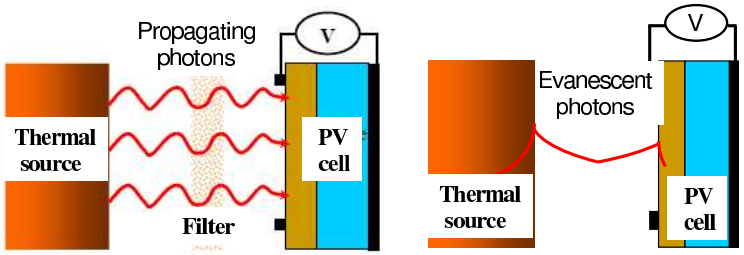

Fig. 14. Principle of thermophotovoltaic energy conversion devices. (a) In far field, the photovotlaic (PV) cell is located at long distance (compared to the thermal wavelength) from a thermal source. Propagating photons only reach the cell. A filter can eventually select the photons with an energy higher than that of the energy gap of the cell. (b) In near-field TPV the cell is located at subwavelength distance from the source. Evanescent photons are the main contributors to the radiative power transfered from the source to the cell.

In far field, this efficiency is in principle limited by the thermodynamic Schockley-Queisser limit (Shockley and Queisser (1961)) wich corresponds to the case where the source is a perfect black body and is typically about 33%. This limit could be easily overcome with a monochromatic source when the frequency of emission coincides with the gap energy of the semiconductor. In this case η would be equal to one. However, first it is difficult to have natural materials with a monochromatic emission so that some photons are generally dissipated incide the cell without participating to the conversion. Second, the production of electricity depends directly on the magnitude of radiative flux received by the cell. But, in the far field, the heat flux cannot exceed that of black body. On the other hand, in the near-field the heat flux can be several orders of magnitude larger than that of a black body, so that near-field TPV conversion (Basu et al. (2009); Laroche et al. (2006); Narayanaswamy and Chen (2003); Pan et al. (2000); Park et al. (2007)) seems to be a promising technology for an intensive production of electricity.

Generaly speaking, in (far or near-field) TPV devices, the maximal power which can be extracted from the cell reads (Laroche et al. (2006))

$$P_{el} = F_{\mathrm{fill}} I_{\mathrm{ph}} V_{\mathrm{oc}}, \tag{47}$$

where I_{ph} is the photogeneration current (which corresponds to photons that are effectively converted), V_{oc} is the open-circuit voltage (which correspond to a vanishing current into the diode). The factor F_{fill} is called fill factor and depends on I_{ph} and on the saturation current I_0 of the diode. When we assume that each absorbed photon with an energy higher than the gap energy E_{g} produces an electron-hole pair, the photogeneration current reads (Laroche et al. (2006))

$$I_{\mathrm{ph}} = e \int_{E_{\mathrm{g}}/\hbar}^{\infty} \mathrm{d}\omega \, \frac{P_{\mathrm{rad}}(\omega)}{\hbar\omega}. \tag{48}$$

It immediately follows from this equation that an increase in the radiative power exchanged between the source and the cell leads to an enhancement of the photogeneration current. On

the other hand, the fill factor is given by (Laroche et al. (2006))

$$F_{\text{fill}} = \left[1 - \frac{1}{\ln(I_{\text{ph}}/I_0)}\right]\left[1 - \frac{\ln(\ln(I_{\text{ph}}/I_0))}{\ln(I_{\text{ph}}/I_0)}\right], \tag{49}$$

with the dark current (Ashcroft and Mermin (1976))

$$I_0 = e\left(\frac{n_i^2 D_{\text{h}}}{N_{\text{D}}\tau_{\text{h}}^{1/2}} + \frac{n_i^2 D_{\text{e}}}{N_{\text{A}}\tau_{\text{e}}^{1/2}}\right). \tag{50}$$

In Eq.(50) n_i denotes the intrinsic carrier concentration, N_D (N_A) the donor (acceptor) concentration, D_{e} (D_{h}) the diffusion constant of electrons (holes) and τ_{e} and τ_{h} represent the electron-hole pair lifetime in the p-doped and n-doped domains of the cell. In Fig. 15 we see that for a plane tungsten thermal source in front of a GaSb cell (see Palik (1998) for optical properties) the radiative power exchanged increases dramaticaly at subwavength distances compared to what we observe in far field. As direct consequence, the photocurrent generated in the GaSb cell follows an analog behavior.

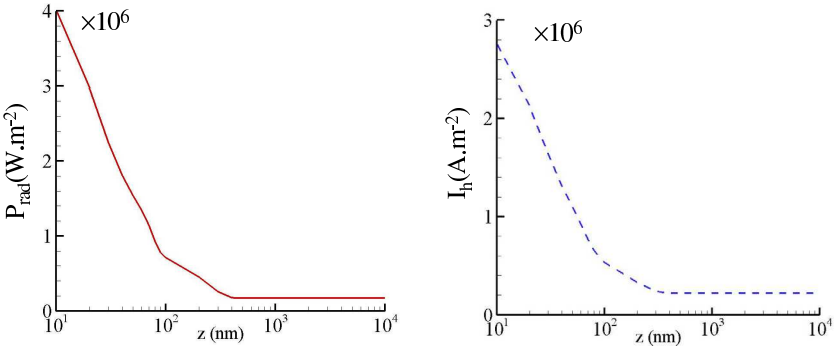

Fig. 15. (a) Radiative power exchanged between a tungsten source at 2000K and a GaSb cell at 300K. (b) Photocurrent in the GaSb cell with respect to the separation distance z of the thermal source. $N_{\text{A}} = N_{\text{D}} = 10^{-17}\text{cm}^{-3}$; $n_i = 4.3 \times 10^1 2\text{cm}^{-3}$. Physical properties are taken from (Rosencher and Vinter (2002))

Once the photocurrent and the dark current are known, the electric power [see Eq. (47)] can be calculated using the open circuit voltage (Laroche et al. (2006))

$$V_{\text{oc}} = \frac{k_{\text{B}}T}{e}\log\left(\frac{I_{\text{h}}}{I_0}\right). \tag{51}$$

Fig. 16 clearly shows that the near-field TPV device produces much more electricity than a classical TPV conversion system. At a distance between the thermal source and the cell of $z = 100nm$ the production is approximatly enhanced by a factor of 5. At 10 nm this factor reaches a value of about 50 times the far-field value. These results show that the near-field TPV conversion is a promising technology that could offer new solutions for energy production in the next decades.

P. B.-A. and F.S.S. R. acknowledge the support of the Agence Nationale de la Recherche through the Source-TPV project ANR 2010 BLANC 0928 01. This research was partially supported by Triangle de la Physique, under the contract 2010-037T-EIEM.

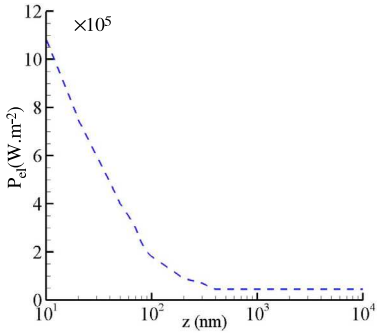

Fig. 16. Electric power generated by a Tungsten-GaSb cell with respect to the separation distance cell-source (same parameters as in (Laroche et al. (2006))).

5. References

G. S. Agarwal (1975), Quantum electrodynamics in the presence of dielectrics and conductors. I. Electromagnetic-field response functions and black-body fluctuations in finite geometries, *Physical Review A*, Vol. 11 (No. 1): 230-242.

N. Ashcroft and N. D. Mermin (1976), *Solid-State Physics*, Harcourt College Publishers, Philadelphia.

G. Baffou, M. P. Kreuzer, and R. Quidant (2009), Temperature mapping near plasmonic nanostructures using fluorescence polarization anisotropy, *Optics Express*, Vol. 17 (No. 5), 3291-3298.

S. Basu and M. Francoeur (2011), Near-field radiative transfer based thermal rectification using doped silicon, *Applied Physical Letters*, Vol. 98: 113106.

S. Basu, Z. M. Zhang, and C. J. Fu (2009), Review of near-field thermal radiation and its application to energy conversion,*International Journal of Energy Research*, Vol. 33 (No. 13), 1203-1232.

S. Basu and Z. M. Zhang (2009), Maximum energy transfer in near-field thermal radiation at nanometer distances, *Journal of Applied Physics*, Vol. 105: 093535.

P. Ben-Abdallah and K. Joulain (2010), Fundamental limits for noncontact transfers between two bodies,*Physical Review B(R)*, Vol. 82 (No. 12): 121419.

S.-A. Biehs, E. Rousseau, and J.-J. Greffet (2010), A mesoscopic description of radiative heat transfer at the nanoscale, *Physical Review Letters*, Vol. 105(No. 23): 234301.

S.-A. Biehs, O. Huth, F. Rüting, M. Holthaus (2010b), Spheroidal nanoparticles as thermal near-field sensors, *Journal of Applied Physics*, Vol. 108 (No. 1): 014312.

S.-A. Biehs and J.-J. Greffet (2010c), Influence of roughness on near-field heat transfer between two plates, *Physical Review B*, Vol. 82 (No. 24): 245410.

S.-A. Biehs and J.-J. Greffet (2010d), Near-field heat transfer between a nanoparticle and a rough surface, *Physical Review B*, Vol. 81 (No. 24): 245414.

S.-A. Biehs, O. Huth, and F. Rüting (2008), Near-field radiative heat transfer for structured surfaces, *Physical Review B*, Vol. 78 (No. 8): 085414.

S.-A. Biehs, F. S. S. Rosa, P. Ben-Abdallah, K. Joulain, and J.-J. Greffet (2011), Nanoscale heat flux between nanoporous materials, *Optics Express*, Vol. 19 (No. S5): A1088-A1103.

S.-A. Biehs, F. S. S. Rosa, and P. Ben-Abdallah (2011b), Modulation of near-field heat transfer between two gratings, *Applied Physical Letters*, Vol. 98: 243102.

R. Carminati and J.-J. Greffet (1999), Near-field effects in spatial coherence of thermal sources, *Physical Review Letters*, Vol. 82 (No. 8): 1660-1663.

P.-O. Chapuis, S. Volz, C. Henkel, K. Joulain, and J.-J. Greffet (2008), Effects of spatial dispersion in near-field radiative heat transfer between two parallel metallic surfaces,*Physical Review B*, Vol. 77: 035431.

P.-O. Chapuis, M. Laroche, S. Volz, and J.-J. Greffet (2008b), Near-field induction heating of metallic nanoparticles due to infrared magnetic dipole contribution, *Physical Review B*, Vol. 77 (No. 12): 125402.

W. C. Chew (1995), *Waves and Fields in Inhomogeneous Media*, IEEE Press.

T. J. Coutts (1999), A review of progress in thermophotovoltaic generation of electricity,*Renewable and Sustainable Energy Reviews*, Vol. 3: 77-184.

E. Cravalho, C. Tien, and R. Caren (1967), Effect of small spacings on radiative transfer between 2 dielectrics, *J. Heat Transfer*, Vol. 89 (No. 4): 351.

S. Datta (2002), *Electronic Transport in Mesoscopic Systems*, Cambridge University Press.

Y. De Wilde, F. Formanek, R. Carminati, B. Gralak, P.A. Lemoine, K. Joulain, J.P. Mulet, Y. Chen and J.J. Greffet (2006), Thermal radiation scanning tunnelling microscopy, Nature (London), Vol. 444: 740-743.

G. V. Dedkov and A. A. Kyasov (2007), Thermal radiation of nanoparticles occurring at a heated flat surface in vacuum, *Technical Physics Letters*, Vol. 33 (No. 4), 305-308.

I. A. Dorofeyev (1998), Energy dissipation rate of a sample-induced thermal fluctuating field in the tip of a probe microscope,*Journal of Physics D: Applied Physics*, Vol. 31 (No. 6): 600-601.

I. A. Dorofeyev and E. A. Vinogradov (2011), Fluctuating electromagnetic fields of solids, *Physics Reports*, Vol. 504 (No. 1-2): 75.

G. W. Ford and W. H. Weber (1984), Electromagnetic interactions of molecules with metal surfaces, *Physics Reports*, Vol. 113 (No. 4): 195-287.

J.-J. Greffet (1988), Scattering of electromagnetic waves by rough dielectric surfaces, *Physical Review B*, Vol. 37 (No. 11): 6436-6441.

C. Henkel and V. Sandoghdar (1998), Single-molecule spectroscopy near structured dielectrics, Optics Communications, Vol. 158: 250-262.

L. Hu, A. Narayanaswamy, X. Chen, and G. Chen (2008), Near-field thermal radiation between two closely spaced glass plates exceeding Planck's blackbody radiation law, *Applied Physics Letters*, Vol. 92 (No. 13), 133106.

O. Huth, F. Rüting, S.-A. Biehs, M. Holthaus (2010), Shape-dependence of near-field heat transfer between a spheroidal nanoparticle and a flat surface, *The European Physical Journal Applied Physics*, Vol. 50 (No. 1): 10603.

F. Huth, M. Schnell, J. Wittborn, N. Ocelic and R. Hillenbrand (2011), Infrared-spectroscopic nanoimaging with a thermal source, *Nature Materials*, Vol. 10: 352-356.

Y. Imry (2002), *Introduction to Mesoscopic Physics*, Oxford University Press.

J. D. Jackson (1998), *Classical Electrodynamics*, 3rd ed., John Wiley, New York.

M. Janowicz, D. Reddig, and M. Holthaus (2003), Quantum approach to electromagnetic energy transfer between two dielectric bodies, *Physical Review A*, Vol. 68 (No. 4): 043823.

K. Joulain, R. Carminati, J.-P. Mulet, and J.-J. Greffet (2003), Definition and measurement of the local density of electromagnetic states close to an interface, *Physical Review B*, Vol. 68 (No. 68), 245405 (2003).

K. Joulain, J.-P. Mulet, F. Marquier, R. Carminati, and J.-J. Greffet (2005), Surface electromagnetic waves thermally excited: Radiative heat transfer, coherence properties and Casimir forces revisited in the near field, *Surface Science Report*, Vol. 57 (No. 3-4): 59-112.

C. Henkel and K. Joulain (2006), Electromagnetic field correlations near a surface with a nonlocal optical response,*Applied Physics B: Lasers and Optics*, Vol. 84 (No. 1-2): 61-68.

Y. Kajihara, K. Kosaka, S. Komiyama (2010), A sensitive near-field microscope for thermal radiation, *Review of Scientific Instruments*, Vol. 81 (No. 3): 033706.

A. Kittel, W. Müller-Hirsch, J. Parisi, S.-A. Biehs, D. Reddig, and M. Holthaus (2005), Near-field heat transfer in a scanning thermal microscope, *Physical Review Letters*, Vol. 95 (No. 22), 224301. 301 (2005).

A. Kittel, U. F. Wischnath, J. Welker, O. Huth, F. Rüting, and S.-A. Biehs (2008), Near-field thermal imaging of nanostructured surfaces, *Applied Physics Letters*, Vol. 93 (No. 19): 193109.

C. Kittel (1962), *Introduction to Solid State Physics*, 2nd ed. John Wiley and Sons, New York.

K. L. Kliewer and R. Fuchs (1974), Theory of dynamical properties of dielectric surfaces, *Advances in Chemical Physics*, Vol. 27: 355-541.

J.A. Kong (2007), *Electromagnetic Wave Theory*, 2nd ed., Wiley.

R. Kubo, M. Toda, and N. Hashitsume (1991),*Statistical Physics II*, 2nd ed., Springer, Berlin Heidelberg.

L.D. Landau, E.M. Lifshitz, and L.P. Pitaevskii (2007), *Electrodynamics of Continuous Media*, 2nd ed. Elsevier, Oxford.

M. Laroche, R. Carminati, and J. J. Greffet (2006), Near-field thermophotovoltaic energy conversion, *Journal of Applied Physics*, Vol. 100: 063704.

E. M. Lifshitz, L. P. Pitaevskii, *Statistical Physics, Part 2*, Butterworth-Heinemann, Oxford.

A. Majumdar, 1999, Scanning thermal microscopy, *Annual Review of Materials Science*, Vol. 29: 505-585.

J.-P. Mulet, K. Joulain, R. Carminati, and J.-J. Greffet (2001), Nanoscale radiative heat transfer between a small particle and a plane surface, *Applied Physics Letters*, Vol. 78 (No. 19): 2931-2933.

W. Müller-Hirsch, A. Kraft, M. T. Hirsch, J. Parisi, and A. Kittel (1999), Heat transfer in ultrahigh vacuum scanning thermal microscopy, *Journal of Vacuum Science & Technology A*, Vol. 17 (No. 4): 1205-1211.

A. Narayanaswamy and G. Chen (2003), Surface modes for near field thermophotovoltaics, *Applied Physics Letters*, Vol. 82: 3544-3546.

A. Narayanaswamy, S. Shen, and G. Chen (2008), Near-field radiative heat transfer between a sphere and a substrate ,*Physical Review B*, Vol. 78 (No. 11): 115303.

T. Ojanen and A.-P. Jauho (2008), Mesoscopic photon heat transistor, *Physical Review Letters*, Vol. 100: 155902 (2008).

C. R. Otey, W. T. Lau, and S. Fan (2010), Thermal rectification through Vacuum, *Physical Review Letters*, Vol. 104: 154301.

R. Ottens, V. Quetschke, S. Wise, A. Alemi, R. Lundock, G. Mueller, D. H. Reitze, D. B. Tanner, B. F. Whiting (2011), Near-Field Radiative Heat Transfer between Macroscopic Planar Surfaces, *Physical Review Letters*, Vol. 107 (No. 1): 014301.

E.D. Palik (1998), *Handbook of Optical Constants of Solids*, Academic Press, London.

J. L. Pan, H. K. H. Choy, C. G. Fonstad (2000), Very large radiative transfer over small distances from a black body for thermophotovoltaic applications, *IEEE Transactions on Electron Devices*, Vol. 47(No. 1): 241 - 249.

K. Park, S. Basu, W. P. King (2007), Z. M. Zhang, Performance analysis of near-field thermophotovoltaic devices considering absorption distribution, *Journal of Quantitative Spectroscopy & Radiative Transfer*, Vol. 109: 305-316.

J. B. Pendry (1983), Quantum limits to the flow of information and entropy, *Journal of Physics A: Mathematical and General*, Vol. 16(No. 10), 2161-2171.

J. B. Pendry (1999), Radiative exchange of heat between nanostructures,*Journal of Physics: Condensed Matter*, Vol. 11 (No. 35): 6621-6634.

T.G. Philbin and U. Leonhardt (2008), Alternative calculation of the Casimir forces between birefringent plates, *Physical Review A*, Vol. 78: 042107

D. Polder and M. Van Hove (1971), Theory of radiative heat transfer between closely spaced bodies, *Physical Review B*, Vol. 4(No. 4): 3303-3314.

H. Raether (1988),*Surface Plasmons on Smooth and Rough Surfaces and on Gratings*, Springer, Heidelberg.

L. G. C. Rego and G. Kirczenow (1999), Fractional exclusion statistics and the universal quantum of thermal conductance: A unifying approach, *Physical Review B*, Vol. 59(No. 20): 13080-13086.

F. S. S. Rosa, D. A. R. Dalvit, and P. W. Milonni (2008), Casimir interactions for anisotropic magnetodielectric metamaterials, *Physical Review A*, Vol. 78: 032117.

F. S. S. Rosa, D. A. R. Dalvit, and P. W. Milonni (2010), Electromagnetic energy, absorption, and Casimir forces: Uniform dielectric media in thermal equilibrium, *Physical Review A*, Vol. 81 (No. 3): 033812.

E. Rosencher and B. Vinter (2002), *Optoélectronique*, Dunod, Paris.

E. Rousseau, A. Siria, G. Jourdan, S. Volz, F. Comin, J. Chevrier, and J.-J. Greffet (2009), Radiative heat transfer at the nanoscale, *Nature Photonics*, Vol. 3: 514-517.

E. Rousseau, M. Laroche, and J.-J. Greffet (2009b), Radiative heat transfer at nanoscale mediated by surface plasmons for highly doped silicon, *Applied Physics Letters*, Vol. 95 (No. 23): 231913.

E. Rousseau, M. Laroche, and J.-J. Greffet (2010), Radiative heat transfer at nanoscale: Closed-form expression for silicon at different doping levels, *Journal of Quantitative Spectroscopy & and Radiative Transfer*, Vol. 111(No. 7-8): 1005-1014.

G. Russakoff (1970), A derivation of the macroscopic Maxwell equations, *American Journal of Physics*, Vol. 38 (No. 10): 1188-1195.

F. Rüting, S.-A. Biehs, O. Huth, and M. Holthaus (2010), Second-order calculation of the local density of states above a nanostructured surface, *Physical Review B*, Vol. 82 (No. 11): 115443.

S. M. Rytov, Y. A. Kravtsov, and V. I. Tatarskii (1989), *Principles of Statistical Radiophysics*, Vol. 3, Springer, New York.

W. Shockley and H. Queisser (1961), Detailed balance limit of efficiency of pĆÄên junction solar cells, *Journal of Applied Physics*, Vol. 32: 510.

A. V. Shchegrov, K. Joulain, R. Carminati, and J.-J. Greffet, 2000, Near-field spectral effects due to electromagnetic surface excitations, *Physical Review Letters*, Vol. 87 (No. 7): 1548-1551.

S. Shen, A. Narayanaswamy, and G. Chen (2009), Surface phonon polaritons mediated energy transfer between nanoscale gaps, *Nano Letters*, Vol. 9 (No. 8), 2909-2913.

C.-T. Tai (1971), *Dyadic Green's Functions in Electromagnetic Theory*, Intext Educational Publishers, Scranton.

R. Tao, Z. Chen, and P. Sheng (1990), First-principles Fourier approach for the calculation of the effective dielectric constant of periodic composites, *Physical Review B* Vol. 41: 2417.

M. S. Tomaš (2002), Casimir force in absorbing multilayers, *Physical Review A*, Vol. 66: 052103.

S. Teitler and B.W. Henvis (1970), Refraction in stratified, anisotropic media, *Journal of the Optical Society of America*, Vol. 60: 830.

L. Tsang, J. A. Kong, K.-H. Ding (2000), *Scattering of Electromagnetic Waves*, John Whiley, New York.

P. J. van Zwol, K. Joulain, P. Ben-Abdallah, J.-J. Greffet, J. Chevrier (2011), Fast heat flux modulation at the nanoscale, *Physical Review B* Vol. 83: 201404(R).

P. J. van Zwol, K. Joulain, P. Ben-Abdallah, J. Chevrier (2011), Phonon polaritons enhance near-field thermal transfer across the phase transition of VO2, *Physical Review B* Vol. 84: 161413(R).

E. A. Vinogradov and I. A. Dorofeyev, Thermally stimulated electromagnetic fields of solids, *Physics Uspekhi*, Vol. 52 (No. 1), 425-459.

A. I. Volokitin and B. N. J. Persson (2007), Near-field radiative heat transfer and noncontact friction, *Review of Modern Physics*, Vol. 79 (No. 4): 1291-1329.

U. F. Wischnath, J. Welker, M. Munzel, and A. Kittel (2008), The near-field scanning thermal microscope, *Review of scientific instruments*, Vol. 79 (No. 7): 073708.

M. Wuttig and N. Yamada (2007), Phase-change materials for rewritable data storage, *Nat. Mat.*, Vol. 6: 824.

Z. M. Zhang (2007), *Nano/Microscale Heat Transfer*, McGraw-Hill, New York.